Temperature-Programmed Desorption (TPD) Thermal Desorption Spectroscopy (TDS)

Sven L.M. Schroeder and Michael Gottfried

June 2002

Temperature-programmed desorption (TPD) techniques are important methods for the determination of kinetic and thermodynamic parameters of desorption processes or decomposition reactions. A sample is heated with a temperature program $\beta(t) = \mathrm{d}T/\mathrm{d}t$ (with the temperature T usually being a linear function of the time t) and the partial pressures of atoms and molecules evolving from the sample are measured, e.g. by mass spectrometry. When experiments are performed using well-defined surfaces of single-crystalline samples in a continuously pumped ultra-high vacuum (UHV) chamber then this experimental technique is often also referred to as thermal desorption spectroscopy (TDS).

In the present experiment you will be

- introduced to the thermodynamics and kinetics of adsorption and desorption phenomena.
- introduced to the operation of ultra-high vacuum equipment.
- introduced to the fundamental properties of low-index single crystal metal surfaces and their preparation.
- required to apply your abilities in transforming datasets with a spreadsheet or scientific plotting program.

1. Fundamental Principles

1.1 Physisorption and Chemisorption

Adsorption takes place when an attractive interaction between a particle and a surface is strong enough to overcome the disordering effect of thermal motion. When the attractive interaction is essentially the result of van-der-Waals forces then physisorption takes place. Physisorptive bonds are characterised by dissociation energies below approximately 50 kJ/mol. Chemisorption occurs when the overlap between the molecular orbitals of the adsorbed particle and the surface atoms permit the formation of chemical bonds, which are characterised by dissociation energies typically exceeding 50 kJ/mol. Note

that chemisorption is often an activated process, *i.e.*, the formation of a chemisorptive bond requires that an activation barrier is overcome. A common feature of molecular chemisorption is the weakening of intramolecular bonds that often lead to the dissociation of the adsorbed molecule. An important example for activated, dissociative chemisorption is the adsorption of oxygen molecules on most metal surfaces at room temperature. The elementary reaction steps occurring during this reaction are summarised in Figure 1.

1.2 Thermodynamic View of Adsorption: The Heat of Adsorption

The temperature dependence of the gas pressure p required for equilibrium between the adsorption and desorption can be calculated with the Clausius-Clapeyron equation. If we assume that equilibrium is defined by a constant ratio Θ between the number N_{ads} of adsorbed particles and the number N_{surf} of adsorption sites available at a surface (in the following, this ratio shall be referred to as the *surface coverage* $\Theta = N_{ads}/N_{surf}$) then the condition for chemical equilibrium between adsorbate and gas phase particles is equality of the chemical potentials of the particles in both phases, *i.e.* $d\mu_{ads} = d\mu_{gas}$. Neglecting the volume of the

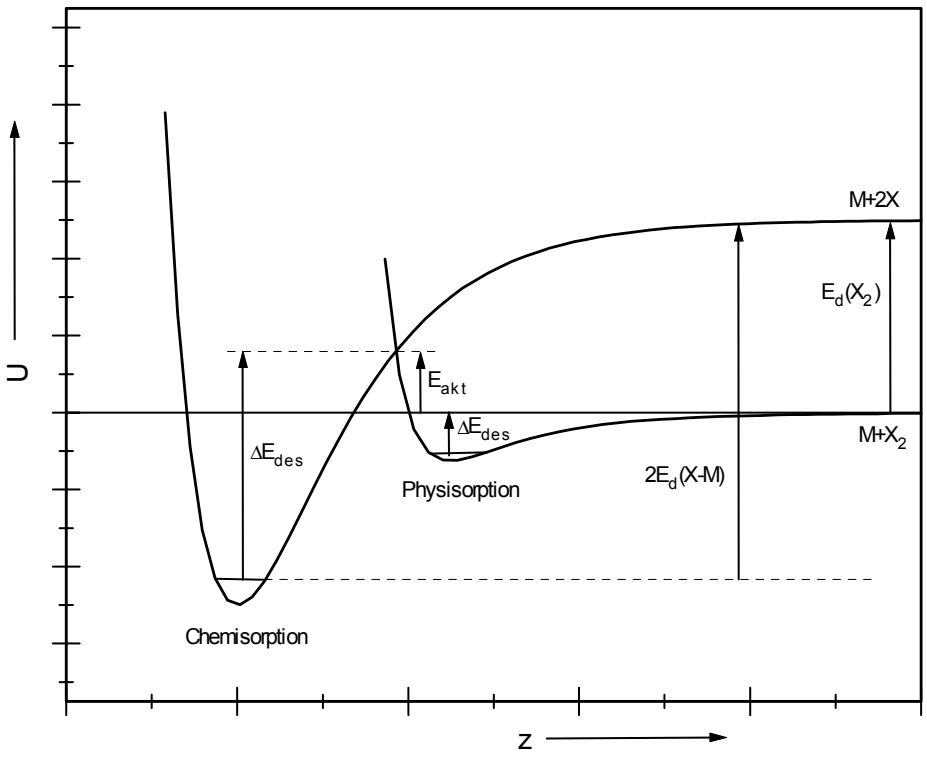

Figure 1 Schematic potential diagram for the activated, dissociative adsorption of a diatomic molecule X_2 that approaches a substrate surface along the trajectory z. The physisorption potential has been assumed to be a *Lennard-Jones* potential, whereas chemisorption is described in this diagram by a *Morse* potential.

condensed surface phase one obtains

$$\left(\frac{\partial \ln p}{\partial T}\right)_{\Theta} = \frac{q_{isost}}{RT^2}. \tag{1}$$

q_{isost} is called the *isosteric heat of adsorption* and is a differential heat, *i.e.*,

$$q_{isost} = (\partial H/\partial \Theta)_T. \tag{2}$$

However, note that alternative definitions for equilibrium can be chosen, which depend on the parameter set used for the characterisation of the adsorption/desorption equilibrium. For example, instead of defining equilibrium by a constant surface coverage one can require a constant pressure ϕ at the surface. In this case we obtain a Clausius-Clapeyron equation that contains a different heat $q_{eq,}$

$$\left(\frac{\partial \ln p}{\partial T}\right)_{\phi} = \frac{q_{eq}}{RT^2} \tag{3}$$

which is now called the *equilibrium heat of adsorption.* It is an integral heat, *i.e*.

$$q_{eq}(\phi) = \int_0^{\phi} dH_T(\phi')d\phi'. \tag{4}$$

Clark has discussed more definitions for the heat of adsorption in his book [4].

1.3 Kinetics of Adsorption and Desorption

1.3.1 Adsorption Isotherms *

Adsorption isotherms describe the surface coverage as a function of the gas pressure over the sample. The most important adsorption isotherm for the discussion of adsorption/desorption phenomena is the *Langmuir* adsorption isotherm [7], which is based on the following assumptions:

- Adsorption is localised, i.e., the adsorbed particles are immobile.
- The substrate surface is saturated at $\Theta = 1$ ML (monolayer), *i.e*., when all adsorption sites are occupied.
- There are no interactions between the adsorbed particles.

In this case, we obtain for the rates of adsorption and desorption

* This section is for information only. It is not required for the analysis of the data acquired during this experiment.

$$r_{ad}(\Theta) = A_n p(1-\Theta)^n \tag{5}$$

$$r_{des}(\Theta) = B_n \Theta^n \qquad (A_n, B_n = \text{const.}, n = 1, 2). \tag{6}$$

From the condition for a dynamic equilibrium $|r_{ad}| = |r_{des}|$ it follows that

$$\Theta_n = \frac{(b_n p)^{1/n}}{1 + (b_n p)^{1/n}} \qquad (b_n = b_n(T) = A_n/B_n = \text{const.}, \quad n = 1, 2). \tag{7}$$

For n = 1 we have a first order rate law for adsorption and desorption. For $n = 2$ we have a second order process, which corresponds, e.g., to dissociative adsorption and recombinative desorption of diatomic molecules. Note that the dissociation of molecules can often be suppressed by lowering the temperature of the surface. An example is the adsorption of O_2 on Ag(110), which is dissociative at room temperature, but non-dissociative ($n = 1$) at 150 K [1].

Other commonly used adsorption isotherms are those of *Freundlich* and of *Brunauer, Emmett* and *Teller* (*BET* isotherm) [2]:

$$\Theta = \alpha \cdot p^{\beta} \qquad \textit{Freundlich} \text{ isotherm}, \quad 0.2 < \beta < 1.0 \tag{8}$$

$$\frac{p}{(p - p_0)\gamma} = \frac{1}{C\gamma_{max}} + \frac{C-1}{C\gamma_{max}} \cdot \frac{p}{p_0} \qquad \textit{BET} \text{ isotherm} \tag{9}$$

p_o ... Vapour pressure of the pure liquid phase at the given temperature

C ... constant specific for the system

γ... adsorption molality, $\gamma = N_{ads}/(m_A \cdot N_L)$

m_A ... mass of one adsorbate particle

γ_{max} ... maximum molality that can be achieved with a monatomic layer.

The *BET* isotherm extends the assumptions of the *Langmuir* isotherm to adsorption in multiple layers. It is assumed that only the first monatomic layer is bound to the substrate surface, whereas all subsequently adsorbed layers are held by the same bonds as those in the liquid phase of the adsorbed molecules. As for the *Langmuir*-isotherm it is assumed that there is no interaction between particles within the same layer. The model is thus describing non-interacting chains of adsorbed particles that grow perpendicular to the surface. In other words, every particle in the chains is assumed to have a coordination number of 2. It is therefore not surprising that, for multilayer coverages, the predictions of *BET* isotherms differ considerably from experimental isotherms. The great practical importance of the *BET* isotherm stems from plotting the left part of equation (9) vs. p/p_0: the intercept with the y-axis and the slope of the

resulting curve provide a value for γ_{max}. If the area covered by an individual adsorbed particle is known then the specific surface area of the substrate material can be determined.

1.3.2 *Polanyi-Wigner* Equation

The principle of microscopic reversibility demands that a reaction passes through exactly the same states irrespective of whether it proceeds forward or backward. Adsorption and desorption can therefore be described by the same set of rate equations. The desorption rate is usually expressed by a rate law of n^{th} order:

$$r_{des} = -\frac{d\Theta}{dt} = k_n \cdot \Theta^n . \tag{10}$$

If the rate constant k_n is described by the *Arrhenius* equation

$$k_n = \nu_n \cdot \exp\left(-\frac{\Delta E_{des}^{PW}}{RT}\right), \tag{11}$$

then the rate law is usually referred to as the *Polanyi-Wigner* equation:

$$r_{des} = -\frac{d\Theta}{dt} = \nu_n \cdot \exp\left(-\frac{\Delta E_{des}^{PW}}{RT}\right) \cdot \Theta^n , \tag{12}$$

which defines the activation energy of desorption ΔE_{des}^{PW} .

1.3.3 Transition State Theory of the Desorption Rate *

The transition state theory is based on the following assumptions:

- States along the reaction coordinate are statistically occupied according to a *Boltzmann* distribution.
- Particles that reach the transition state (≠) will always pass over it.

With these assumptions, a desorption reaction can be described by the following two-step reaction

$$n \cdot X_{ad} \longrightarrow Y_{ad}^{\neq} \longrightarrow Z_{gas} . \tag{13}$$

The overall rate r_{des} can then be written as

---

* This section is background information only. It will not be required for the analysis of the data acquired in this experiment.

$$r_{des} = \frac{\frac{1}{2}[Y_{ad}^{\neq}]}{\tau}, \tag{14}$$

wherein τ is the time spent in the transition state, which is given by

$$\tau = \frac{\delta}{\bar{v}} = \delta \cdot \left(\frac{\pi m^{\neq}}{2kT} \right)^{1/2}, \tag{15}$$

Here, δ is the part of the reaction coordinate (in units of a length) where the activated complex of mass $m^{\neq}$ exists ($\bar{v}$ is its mean translational velocity – see below for more details).

To determine the concentration of activated complexes [$Y_{ad}^{\neq}$] we now consider the equilibrium between adsorbate and transition state:

$$K = \frac{[Y_{ad}^{\neq}]}{[X_{ad}]^n} \tag{16}$$

and include $[X_{ad}] = N_A \cdot \Theta$ as the rate of desorption

$$r_{des} = \frac{1}{2\tau} \cdot K \cdot [X_{ad}]^n = \frac{1}{2\tau} \cdot K \cdot N_A^n \cdot \Theta^n . \tag{17}$$

This expression corresponds to the *Polanyi-Wigner* equation (12) with a rate constant

$$k_n = \frac{1}{2\tau} \cdot K \cdot N_A^n . \tag{18}$$

The equilibrium constant K is statistically calculated from a *Boltzmann* distribution. The general expression for the statistical rate constant is:

$$K = \prod_i z_i^{\nu_i} \cdot \exp\left(-\frac{\Delta E}{RT} \right), \tag{19}$$

where ΔE represents the difference between the ground state energies of reactants and products, which are thus included in the calculation relative to the same zero point of the energy scale.

The activated reaction complex moves along the reaction coordinate in an approximately constant (*i.e.*, not harmonic) potential, so that its movement must be described by a translational degree of freedom. To account for this we remove one vibrational degree of freedom from the partition function $Z^{\neq}$ of the activated complex and add a translational degree of freedom. The partition function for this translational degree of freedom is

$$z_{tr}^{\neq} = (2\pi m^{\neq} kT)^{1/2} \cdot \frac{\delta}{h}, \tag{20}$$

so that the partition function of the activated complex becomes

$$z^{\neq} = z_{-vib}^{\neq} \cdot z_{tr}^{\neq} = z_{-vib}^{\neq} \cdot (2\pi m^{\neq} kT)^{1/2} \cdot \frac{\delta}{h} \tag{21}$$

For the case of desorption the equilibrium constant is therefore

$$K = \frac{z^{\neq}}{z_{ad}^{n}} = \frac{1}{z_{ad}^{n}} \cdot z_{-vib}^{\neq} \cdot (2\pi m^{\neq} kT)^{1/2} \cdot \frac{\delta}{h} \cdot \exp\left(-\frac{\Delta E_{des}^{TST}}{RT}\right), \tag{22}$$

with ΔE_{des}^{TST} being the activation energy for desorption predicted by the transition state theory. Comparing with (18) provides for the reaction rate constant k_n

$$k_n = \frac{K \cdot N_A^n}{2\tau} = \frac{kT}{h} \cdot N_A^n \cdot \frac{z_{-vib}^{\neq}}{z_{ad}^{n}} \cdot \exp\left(-\frac{\Delta E_{des}^{TST}}{RT}\right) \equiv \frac{kT}{h} \cdot K^{\neq}, \tag{23}$$

The expression on the right side of (23) can be seen as the product between the frequency factor kT/h and an equilibrium constant $K^{\neq}$, which is, except for the missing degree of freedom of the reaction coordinate, identical to the equilibrium constant K.

To extract thermodynamic quantities for the activation process we now define an arbitrary width δ of the transition state (i.e., the length along the reaction coordinate where the activated complex of mass $m^{\neq}$ exists - see above!) according to

$$(2\pi m^{\neq} kT)^{1/2} \cdot \frac{\delta}{h} \equiv 1. \tag{24}$$

Accepting this expression is equal to assuming that $z^{\neq} \equiv 1$ for the translational partition function, for which we obtain

$$K^{\neq} = K = \frac{[Y_{ad}^{\neq}]}{[X_{ad}]^{n}}, \tag{25}$$

i.e., the equilibrium constant $K^{\neq}$ can now be regarded as the equilibrium constant K for the first reaction in (13). The free enthalpy of activation $\Delta G^{\neq}$ can now be calculated according to

$$K = \exp\left(-\frac{\Delta G_{des}^{\neq}}{RT}\right), \tag{26}$$

and the rate constant k_n can be interpreted with thermodynamic quantities according to

$$k_n = \frac{kT}{h} \cdot \exp\left(-\frac{\Delta G_{des}^{\neq}}{RT}\right) = \frac{kT}{h} \cdot \exp\left(\frac{\Delta S_{des}^{\neq}}{R}\right) \cdot \exp\left(-\frac{\Delta H_{des}^{\neq}}{RT}\right). \tag{27}$$

Note that we have so far encountered three activation energies of desorption, namely ΔE_{des}^{PW}, ΔE_{des}^{TST} and $\Delta H_{des}^{\neq}$, which are *not* identical because the frequency factors in the corresponding pre-exponential terms have a different temperature dependence. However, the differences are in practice often negligible - if only because they are lost in measurement inaccuracies or because the model assumptions for interpreting desorption spectra are insufficient. Usually we can thus make the assumption that $\Delta E_{des}^{PW} \approx \Delta H_{des}^{\neq}$, and the preexponential ν_n in the *Polanyi-Wigner* equation (12) can be set equal to the entropy term in (27), namely

$$\nu_n \approx \frac{kT}{h} \cdot \exp\left(\frac{\Delta S_{des}^{\neq}}{R}\right), \tag{28}$$

from which follows that

$$\Delta S_{des}^{\neq} \approx R \cdot \ln \frac{\nu_n \cdot h}{kT}. \tag{29}$$

This shows that the entropy of desorption can be extracted from the frequency factor.

2. Experimental

2.1 Ultrahigh Vacuum (UHV) Chamber

The UHV system consists of a pumping system and the vacuum vessel. A schematic drawing of the UHV apparatus for this experiment and all devices mounted in it is shown in Figure 2.

All parts of the vacuum vessel are made from high-grade steel. All mountable parts are attached using standard Conflat flanges, which have a knife edge that affords a seal by cutting into an oxygen-free high-conductivity (OFHC) copper ring ("gasket"). Besides the pressure gauge described above, the following equipment is attached to the chamber and will be utilised for the experiment.

- A leak valve, allowing the controlled dosing of gases into the UHV chamber.

- A manipulator onto which a sample can be mounted for studies of its surface properties.
- An ion gun, used for cleaning the surface of the sample by bombardment with ions accelerated to kinetic energies of aproximately 1 keV ("sputtering").
- A quadrupole mass spectrometer.

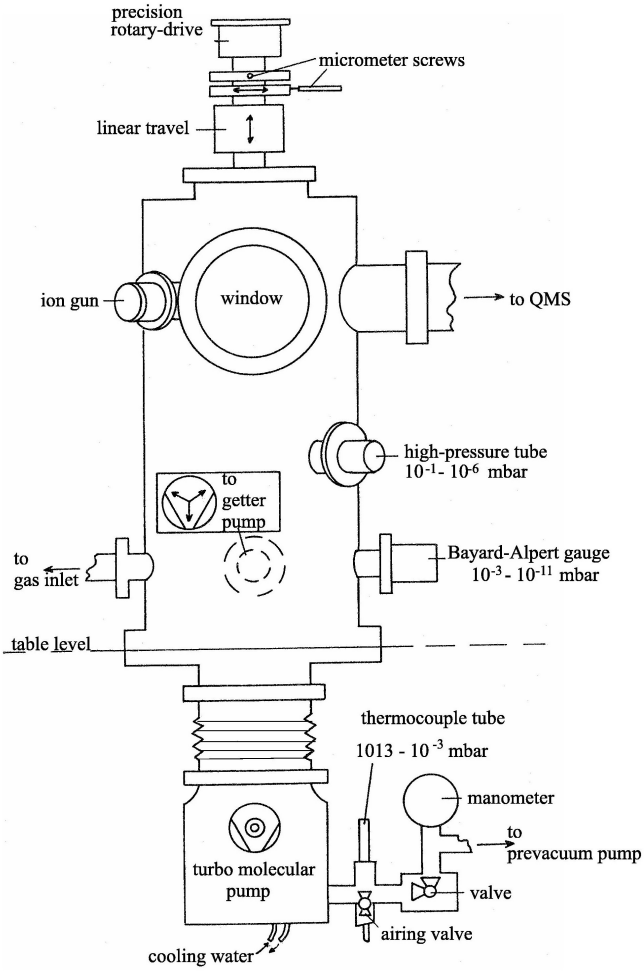

Figure 2 The ultrahigh vacuum apparatus used for this experiment.

2.2 Vacuum Generation and Pumping Speed

Vacuum is maintained by a turbomolecular pump ("turbo") backed by a rotary oil pump. A turbomolecular pump consists of a cylindrical case with stator blades and rotor blades turning at very high speeds (typically in the range of 50,000~rotations/min.). If a gas particle from the vacuum chamber enters the inlet of the pump it collides with a rotor blade and its momentum vector is changed towards the outlet of the pump. It is then removed from the vacuum vessel by a succession of such collision events until it reaches the outlet of the turbomolecular pump.

There it encounters the suction action of a rotary pump that maintains a pressure of approximately 10^{-3} mbar.

2.3 Pressure Measurement

In the ultra-high and high vacuum ranges (up to approximately 0.001 mbar), the pressure is most conveniently and accurately measured by means of a Bayard-Alpert ionisation gauge (fig. 3). It consists of a glowing filament, a grid cage (anode) and the target electrode (cathode). The filament is made of tungsten wire and is resistively heated to a temperature above 2500ºC (white heat). At this temperature electrons are emitted, which ionise gas particles in the environment of the filament. The cations generated by this process are accelerated into the grid cage where they are collected by a target electrode biased at a potential of approximately 600 V. The resulting ion current at the collector is a measure of the pressure. Quantitatively, the pressure p depends on the ion current I_c at the collector and the emission current I_{em} of the filament according to

$$I_c = S\ p\ I_{em}$$

Here, the sensitivity S [$mbar^{-1}$] is a quantity that depends on the gas and the apparatus used. It is tabulated for common gases.

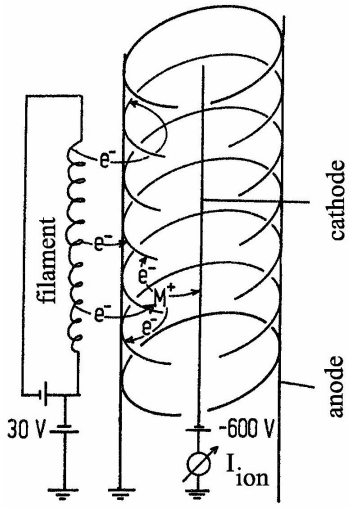

Figure 3 Schematic drawing of a Bayard-Alpert pressure gauge (“ion gauge”).

For pressures exceeding 10^{-3} mbar other types of pressure gauges must be employed: most of these are based on the measurement of the resistance of a thin wire (Pirani gauges), which depends on the heat conductivity of the medium in its environment. The better the vacuum around the wire the lower the heat conductivity of the environment, resulting in a warmer wire with a higher resistance. A variation of this principle is the thermocouple gauge. It is based on a measurement of the thermovoltage at a metal-metal junction, which also depends on the heat conductivity of its surroundings.

2.4 Dosing of Gases

Dosing of gases into the chamber is achieved by use of a leak valve. The final pressure p_f measured during dosing is the sum of the base pressure p_0 and the partial pressure p_i of the gas flowing into the system, *i.e.*, $p_f - p_0 = p_i$ (or $p_i = p_f$ for $p_0 << p_f$).

The partial pressure p_i is proportional to the particle number n_i. In UHV studies of adsorption the unit Langmuir (1 L = 10^{-6} torr s) is used to describe the amount of gas dosed into the system, *i.e.*, 1 L is the gas dose that corresponds to a pressure increase to 10^{-6} torr (760 torr = 101.325 kPa) for 1 s. The number of gas-surface collisions during such a pressure burst is of the same order of magnitude as the number of surface atoms (see section 4).

2.5 Sample Manipulation and Mounting

The sample manipulator is based on a rotatable rod that can be moved horizontally (x,y-plane) and vertically along its z-axis. The manipulator also has electrical feedthroughs with ceramic insulation for connecting crystal mounting wires to a power supply for resistive heating and two thermocouple wires to a temperature controller. A sketch of the manipulator assembly is given in Figure 4. Movement of the manipulator rod is possible through use of special vacuum-tight bellows that are made from stainless steel. Micrometer screws allow the accurate positioning of the crystal.

The sample is mounted on 0.2 mm – 0.4 mm diameter W- or Ta-wires that are supported by Cu-rods, the top of which is attached to a ceramic block. Use of the ceramic block affords electrical insulation of the Cu rods, so that high currents (max. 40 A) can be passed through them to heat the mounting wires resistively. Temperatures of up to approximately 1700 K can thus be obtained at the single crystal sample. The heating power is regulated by a temperature controller that reads the voltage of a thermocouple welded to the side of the single crystal sample.

2.6 Sample Preparation

The sample is not only subjected to contamination by interaction with particles in the background pressure of the vacuum chamber, but also by segregation of crystal impurities. Particularly troublesome are usually non-metallic contaminants in the crystal lattice, such as carbon, oxygen and sulphur. While contaminants from the gas phase can often be removed by gentle heating of the sample, segregated contaminants must often be removed by a different method. Often used are so-called sputter-heat cycles: the carbidic, oxidic or sulphidic contaminants at the surface are first removed by bombardment of the surface with ions (Ne^+, Ar^+ or Kr^+ are the most common choice) accelerated to kinetic energies between 500 eV and 2000 eV. On impact with the sample surface the momentum of the ions is transferred to lattice

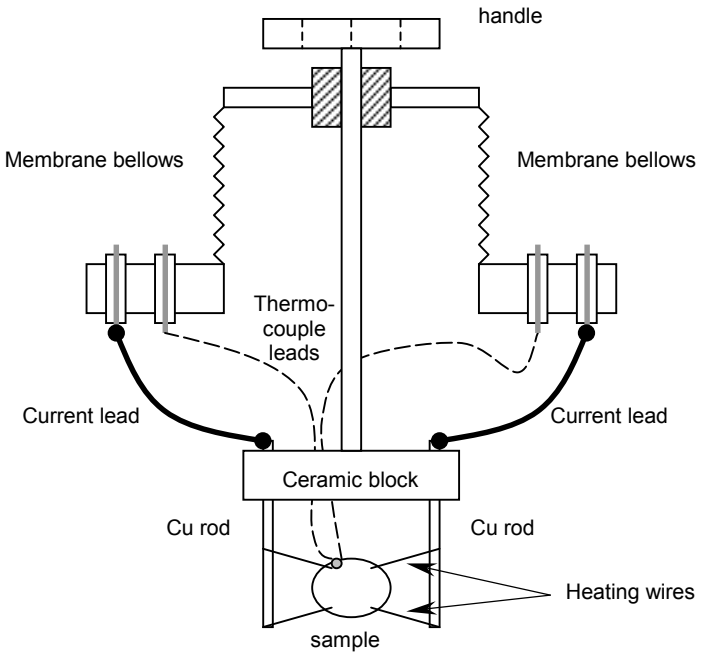

Figure 4 Sketch of the sample manipulator

vibrations in the surface region. This leads to the breaking of bonds to and between surface atoms and the removal of surface atoms layer-by-layer.

2.7 Quadrupole Mass Spectrometer (QMS)

The QMS consists of three components, (i) the ion source with electron impact ioniser and ion extraction optics, (ii) the actual quadrupole analyser consisting of four cylindrically rods, and (iii) the ion detector (electron multiplier). In the present experiment, the ions are generated by electron impact ionisation (as in most conventional mass spectrometers). Free electrons are formed by *thermal emission* from an electrically heated tungsten filament. Thermal electron emission can be described by the Richardson-Dushman equation

$$J = C \cdot \exp\left(- \frac{\Phi}{\mathrm{kT}} \right) \tag{30}$$

with J the current density of emitted electrons, C a constant (independent of the filament material), T the temperature and Φ the work function of the filament material. It is intuitive to see that the emission current increases with the temperature.

The emitted electrons are accelerated by a potential difference (typically 70 V) between the filament and the grid (Figure 5). Ionisation takes place in the area between grid and aperture, which are at approximately equal potentials. The temperature of the filament is in the range around 2500 K. The emitted electrons have a certain kinetic energy distribution due to the

temperature of the filament, but also (more important) due to the electrical potential drop across the heated filament. The energy distribution is typically in the range 2 eV.

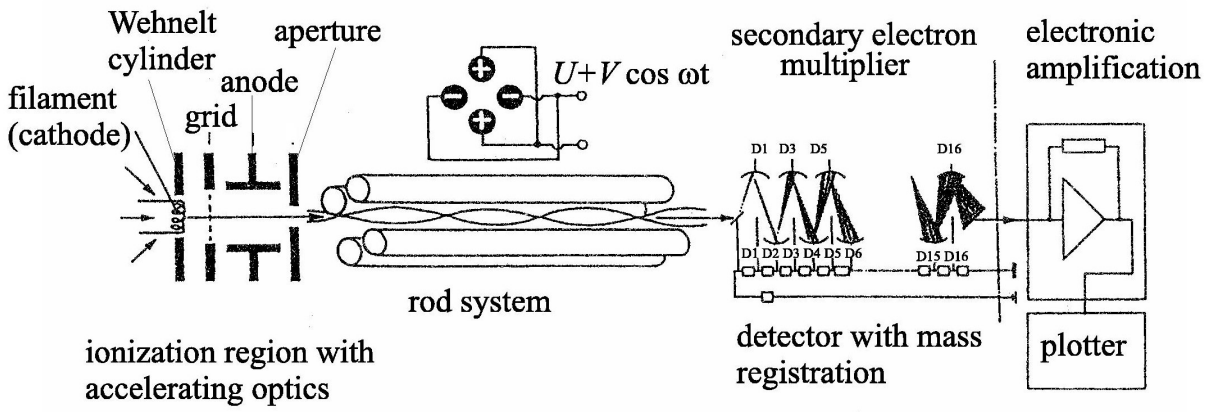

Figure 5 Parts of a quadrupole mass spectrometer.

The quadrupole analyser consists of four cylindrical rods, arranged symmetrically at a distance $r_0(x,y)$ around the optical axis z of the system. Opposite rods are electrically connected. The voltage applied to the two pairs of opposite rods can be expressed as

$$V_1 = U + V \cdot \cos(\omega \cdot t) \tag{31}$$

$$V_2 = -(U + V \cdot \cos(\omega \cdot t)) \tag{32}$$

with a constant component U and a radiofrequency component $V \cdot \cos(\omega \cdot t)$.

In the (x,y)-plane (perpendicular to the quadrupole axis) the potential at any point between the rods is

$$\Phi(x,y) = \frac{(U + V \cdot \cos(\omega \cdot t)) \cdot (x^2 - y^2)}{r_0^2} \tag{33}$$

The differential equations of motion for an ion in such a potential are known as *Mathieu equations*. Their analysis reveals that for a given ion (m/Ze) only certain values of U and V result in stable oscillatory trajectories, while for other values for U and V the amplitude of the oscillations increases exponentially, so that the ion will strike a rod and lose its charge [10].

Note that particles are separated according to their mass/charge ratio m/Ze; doubly ionised paticles thus appear in the spectrum at half their molecular mass, triply charged ions at one third, etc. By this method, molecules with molecular masses of over 1000 can be detected even if the mass spectrometer has a maximum range of, e.g., 300 amu. Apart from the isotope pattern of the molecular ion one can also observe products of ion fragmentation processes.

The simplest way of detecting ions or electrons is *via* the detection of their charges. In simple quadrupole mass spectrometers the ions hit a metallic collector cone (Faraday cup) and the charge transferred is recorded using an electrometer preamplifier, which can detect currents down to a the pA-range. For even lower ion currents (*i.e.*, for less than 10^7 ions per second), one uses secondary electron multipliers or *channeltron* multipliers. Interpretation of Thermal Desorption Spectra

2.8 General Remarks

Spectral interpretation is most commonly performed by use of the *Polanyi-Wigner* equation, as described in section 1.3. An important condition for the determination of accurate data with this equation is that the monitored desorption signal (in the present case, the mass spectrometer signal) is proportional to the rate of desorption. For experiments in UHV this is only the case if the pumping speed is constant and sufficiently high to prohibit significant re-adsorption of desorbed particle on the sample. Furthermore, one elementary step of the desorption process must be rate-limiting, *i.e.*, it must be much slower than all other elementary reactions involved. The activation parameters (frequency factor ν_n, activation energy ΔE^{PW} and desorption order n) provided by the *Polanyi-Wigner* analysis are then only applicable to this rate-limiting step. For example, often the desorption process itself is not rate-limiting but the rate of a reaction preceding it, e.g., slow recombination of atoms to a molecule that quickly desorbs subsequently. In this case, reaction orders higher than 1 can be observed. Note also that the activation parameters are usually dependent on the surface coverage, so that the *Polanyi-Wigner* equation is expressed as

$$r_{des} = -\frac{d\Theta}{dt} = \nu_n(\Theta) \cdot \exp\left(-\frac{\Delta E_{des}^{PW}(\Theta)}{RT}\right) \cdot \Theta^{n(\Theta)}. \tag{34}$$

The activation parameters can also depend on the temperature itself and thus on the heating rate β, *i.e.*, one of the experimental parameters. This is not too surprising as thermal desorption is a dynamic method that provides information on the adsorbate far away from its equilibrium at temperatures below the desorption temperature. As a consequence, the Polanyi-Wigner equation can be an insufficient tool for the analysis of complex desorption data. Modern alternatives to the interpretation by means of the Polanyi-Wigner equation are based on the simulation of desorption spectra with complex statistical models for the interactions experienced by the adsorbate. Often so-called *Monte-Carlo* simulations are used [8].

2.9 Heating Rate Variation Method

This method is based on the collection of a series of spectra for the same adsorbate coverage employing different heating rates $\beta = dT/dt$ = const. From each spectrum, the temperature of the desorption rate maximum $T_{max} = T(\max r_{des})$ is determined. A plot of $\ln\left(T_{max}^2/\beta\right)$ vs. $1/T_{max}$ provides the activation parameters, as follows.

First we substitute the time t in the *Polanyi-Wigner* equation (34) by $dt = (1/\beta)\cdot dT$:

$$\frac{d\Theta}{dT} = -\frac{1}{\beta}\cdot\nu_n\cdot\exp\left(-\frac{\Delta E_{des}^{PW}}{RT}\right)\cdot\Theta^n \tag{35}$$

For the maximum at $T = T_{max}$ the condition

$$\left.\frac{dr_{des}}{dT}\right|_{T_{max}} = 0 \tag{36}$$

must be fulfilled, or, because of $r_{des} = -\frac{d\Theta}{dt} = -\beta\cdot\frac{d\Theta}{dT}$:

$$0 = \left.\frac{d^2\Theta}{dT^2}\right|_{T_{max}} = n\cdot\Theta^{n-1}\cdot\frac{d\Theta}{dT} + \Theta^n\cdot\frac{\Delta E_{des}}{RT_{max}^2}. \tag{37}$$

Inserting (35) for $d\Theta/dT$ and solving for $\Delta E_{des}/RT_{max}^2$ provides

$$\frac{\Delta E_{des}}{RT_{max}^2} = \frac{1}{\beta}\cdot\nu_n\cdot n\cdot\Theta^{n-1}\cdot\exp\left(-\frac{\Delta E_{des}}{RT_{max}}\right). \tag{38}$$

If 1st order desorption ($n = 1$) takes place then T_{max} is independent of the coverage Θ, but dependent on the heating rate β:

$$\frac{\Delta E_{des}}{RT_{max}^2} = \frac{1}{\beta}\cdot\nu_1\cdot\exp\left(-\frac{\Delta E_{des}}{RT_{max}}\right). \tag{39}$$

Taking the logarithm and rearrangement yields

$$\ln\frac{\widetilde{T}_{max}^2}{\widetilde{\beta}} = \frac{\Delta E_{des}}{RT_{max}} + \ln\frac{\Delta\widetilde{E}_{des}}{\widetilde{\nu}_1\cdot\widetilde{R}}. \tag{40}$$

(each logarithmic parameter has been divided by its own unit, i.e., $\widetilde{T} \equiv T/K$ etc.). Plotting of $\ln\left(\widetilde{T}_{max}^2/\widetilde{\beta}\right)$ vs. $1/T_{max}$ for a series of β-values thus provides ΔE_{des} from the slope ν_1 from the intercept with the ordinate.

For 2nd order (n = 2) desorption we obtain from (38) that

$$\frac{\Delta E_{des}}{RT_{max}^2} = \frac{2}{\beta}\cdot\nu_2\cdot\Theta(T_{max})\cdot\exp\left(-\frac{\Delta E_{des}}{RT_{max}}\right). \tag{41}$$

Because desorption states of 2nd order are symmetric with respect to T_{max} we know that $\Theta(T_{max})$ is half the value before desorption, *i.e.*, $\Theta_0 = 2\cdot\Theta(T_{max})$. After division by the units and rearranging we thus obtain

$$\ln\frac{\widetilde{T}_{max}^2}{\widetilde{\beta}} = \frac{\Delta E_{des}}{RT_{max}} + \ln\frac{\Delta\widetilde{E}_{des}}{\widetilde{\nu}_2\cdot\widetilde{R}\cdot\Theta_0}. \tag{42}$$

Plotting of $\ln\left(\widetilde{T}_{max}^2/\widetilde{\beta}\right)$ vs. $1/T_{max}$ as a function of the heating rate β provides ΔE_{des} from the slope and, if Θ_0 is known, the frequency factor ν_2 from the intercept.

2.10 *Analysis According to* Redhead

Redhead [11] derived a simple relation between ΔE_{des}, ν_1 and T_{max}. he assumed that activation parameters are independent of surface coverage and that desorption followed 1st order kinetics. Solving (39) for ΔE_{des} provides

$$\Delta E_{des} = RT_{max}\left[\ln\frac{\nu_1\cdot T_{max}}{\beta} - \ln\frac{\Delta E_{des}}{RT_{max}}\right] \tag{43}$$

The second part in brackets is small relative to the first and is estimated as $\ln(\Delta E_{des}/RT_{max}) = 3.64$. The error introduced through this estimate is less than 1.5% for $10^8 < \nu_1/\beta < 10^{13}\ \mathrm{K}^{-1}$.

The Redhead method is often employed to extract activation energies from a single desorption spectrum. This requires that an approximate value for ν_1 is known. $\nu_1 = 10^{13}\ \mathrm{s}^{-1}$ is a commonly chosen value.

*2.11 Leading Edge Analysis **

This method was introduced by *Habenschaden* and *Küppers* [6] and allows the determination of coverage- and temperature-dependent activation parameters. To keep T and Θ constant a small section of the spectrum on its leading edge is selected. This part of the spectrum is then plotted as $\ln \tilde{r}_{des}$ vs. $1/T$, according to the logarithmic *Polanyi-Wigner* equation

$$\ln \tilde{r}_{des} = -\frac{\Delta E_{des}}{RT} + \ln \tilde{\nu}_n + n \cdot \ln \tilde{\Theta}, \tag{44}$$

From the slope of this *Arrhenius* plot ΔE_{des} can be determined. From the intercept with the ordinate the frequency factor ν_n can be determined provided that reaction order and coverage are known.

The great advantage of this method is that it requires a minimum of assumptions. A drawback is the use of the leading edge for the analysis because the signal/noise ratio in this region of low desorption rates is inherently low.

Closer examination of the method reveals that exact determination of the frequency factor is possible only under certain conditions. To show this we differentiate eq. (34) for $n = 1$ at $T = T_{max}$ with respect to T and take account of the fact that the activation parameters are coverage dependent:

$$\begin{aligned} \left.\frac{d^2\Theta}{dT^2}\right|_{T_{max}} &= 0 \\ &= \frac{d}{dT}\left[-\frac{\nu_1}{\beta}\cdot\exp\left(-\frac{\Delta E_{des}}{RT}\right)\cdot\Theta\right]_{T_{max}} \\ &= \left[-\frac{d\nu_1}{d\Theta}\cdot\frac{d\Theta}{dT}\cdot\Theta + \nu_1\cdot\frac{\Delta E_{des}}{RT^2}\cdot\Theta - \frac{\nu_1\cdot\Theta}{RT}\cdot\frac{d\Delta E_{des}}{d\Theta}\cdot\frac{d\Theta}{dT} + \nu_1\cdot\frac{d\Theta}{dT}\right] \end{aligned} \tag{45}$$

Replacing all occurrences of $d\Theta/dT$ with eq. (35) and assuming $n = 1$ yields

$$0 = \left[\left(\frac{d\nu_1}{d\Theta}\cdot\Theta + \nu_1 - \frac{\nu_1\cdot\Theta}{RT}\cdot\frac{d\Delta E_{des}}{d\Theta}\right)\cdot\left(\frac{1}{\beta}\cdot\exp\left(-\frac{\Delta E_{des}}{RT}\right)\right) - \frac{\Delta E_{des}}{RT^2}\right]_{T_{max}}. \tag{46}$$

Separating all terms that contain ν_1 gives

---

* This section is for information only. You will not be required to use this method for the analysis of the data acquired during this experiment.

$$\frac{\beta \cdot \Delta E_{des}}{RT^2} \cdot \exp\left(\frac{\Delta E_{des}}{RT}\right) = \nu_1 + \Theta \cdot \frac{d\nu_1}{d\Theta} - \frac{\nu_1 \cdot \Theta}{RT} \cdot \frac{d\Delta E_{des}}{d\Theta} . \tag{47}$$

In two cases ν_1 can be determined directly:

- When ΔE_{des} and ν_1 are independent of Θ then the right of eq. (47) simplifies to ν_1.
- When the last two terms on the right of eq. (47) compensate each other, *i.e.*, when

$$\Theta \cdot \frac{d\nu_1}{d\Theta} - \frac{\nu_1 \cdot \Theta}{RT_{max}} \cdot \frac{d\Delta E_{des}}{d\Theta} = 0 \tag{48}$$

Then again ν_1 is equal to the left side of (47) and can be easily determined. It is worthwhile noting that eq. (48) can be rearranged to

$$d \ln \nu_1 = \frac{d\Delta E_{des}}{RT_{max}}, \tag{49}$$

which states that the logarithmic frequency factor scales linearly with the desorption energy. This result is an expression of the so-called *compensation effect*, *i.e.* the frequent observation that an increase in the exponential term in the Arrhenius equation is accompanied by a decrease of the frequency factor.

Generally, for small coverages ($\Theta \to 0$) ν_1 can always be determined accurately because then the two last terms on the right side of (47) vanish as well.

2.12 Plots of $\ln\left(\tilde{r}_{des}/\tilde{\Theta}^n\right)$ vs. $1/T$

The whole desorption spectrum can be rearranged to an *Arrhenius* plot of the form $\ln\left(\tilde{r}_{des}/\tilde{\Theta}^n\right)$ vs. $1/T$ for various values of n, e.g. $n = 0, 1, 2$. Assuming that the Polanyi-Wigner equation holds and that the activation parameters are independent of temperature and coverage then a straight line should be obtained for the correct choice of n. Furthermore, because

$$\ln \frac{-d\tilde{\Theta}/dt}{\tilde{\Theta}^n} = -\frac{\Delta E_{des}}{RT} + \ln \tilde{\nu}_n \tag{50}$$

the activation energy ΔE_{des} can be determined from the slope and the frequency factor ν_n from the intercept with the ordinate. If another order $m \neq n$ is chosen instead of the correct order n then we obtain the following expression:

$$\ln\frac{-d\tilde{\Theta}/dt}{\tilde{\Theta}^m} = \ln\left[\frac{1}{\tilde{\Theta}^m}\cdot\tilde{\nu}_n\cdot\tilde{\Theta}^n\cdot\exp\left(-\frac{\Delta E_{des}}{RT}\right)\right] = (n-m)\cdot\ln\tilde{\Theta} + \ln\tilde{\nu}_n - \frac{\Delta E_{des}}{RT}. \qquad (51)$$

The right side of this equation contains a term $\propto \ln\tilde{\Theta}$, which does not increase linearly with $1/T$, especially in the region of $1/T_{max}$. The resulting plot is concave for $m < n$, and convex for $m > n$.

3. Instructions for the Experiment

- Examine the apparatus and identify the various devices attached to it. Convince yourself that the pressure in the chamber is in the 10^{-9} mbar range or lower.
- Clean the single crystal surface in the chamber by two cycles of 30 min Ar^+-sputtering followed by heating the crystal to restore surface order (the instructor will provide you with exact conditions for these procedures).
- Collect TPD spectra for a CO dose of 0.5 L as a function of the heating rate. Use heating rates of 20 K/s, 10 K/s, 5 K/s, 1 K/s and 0.5 K/s. Analyse the results with the method described in section 2.9.
- Collect a series of TPD spectra for the following doses of CO (complete the table below before you start the experiments!). Use a heating rate of 5 K/s. Repeat the experiments for gas doses of 0.06 L, 0.36 L and 1.00 L so that you can estimate the experimental error.

Dose [L]	**0.03**	**0.06**	**0.09**	**0.18**	**0.27**	**0.36**	**0.50**	**0.75**	**1.00**	**1.50**	**2.00**	**5.00**
Dosing Time [s]	6	12	18	20	20	20	20	20	20	20	20	50
Pressure [torr]	$5\cdot10^{-9}$	$5\cdot10^{-9}$	$5\cdot10^{-9}$						$5\cdot10^{-8}$		$1\cdot10^{-7}$	$1\cdot10^{-7}$
Pressure [mbar]												

- Determine activation energies and preexponential factors for this series using the analysis methods described in sections 2.10 and 2.12. Compare and discuss the results.

4. Questions

There are several excellent textbooks on surface chemistry [3,8,9] for further reading. Many of the standard physical chemistry textbooks in the library also contain enough information to answer these questions.

1. Sketch the arrangement of surface atoms at an fcc(100), fcc(110), fcc(111), hcp(100), hcp(110), hcp(111), bcc(100), bcc(110) and bcc(111) surface. Draw the arrangement of surface and second layer atoms on the single crystal surface that the instructor has provided for the experiment, and include the direction vectors in your drawing.
2. At which pressure [Pascal, Torr] is the frequency of collision between nitrogen molecules in a 1 dm^3 spherical container at T = 0°C equal to the rate of collisions with the walls of the container? Assume for your calculation that nitrogen has a molecular diameter *d* od $3.8 \cdot 10^{-10}$ m. The surface collision rate is

$$Z = \frac{N_{Stoß}}{A \cdot t} = \frac{1}{4} \cdot {}^1N \cdot \bar{c} = pN_L \cdot \sqrt{\frac{1}{2\pi RTM}}, \tag{52}$$

   with ${}^1N$ being number of molecules per volume unit and $\bar{c}$ being the mean molecular velocity. Show how this formula can be derived (consult, e.g., G. Wedler, 1st ed. 1982, chapter 4.3.2, page 678).
3. What surface coverage θ is expected for gas doses of 1 L H_2, O_2, CO and I_2 at 300 K. Assume that each surface collision of a molecule leads to adsorption and that the surface has $3.178 \cdot 10^{15}$ adsorption sites per cm^2. Assume for your calculation that H_2, O_2 und I_2 adsorb dissociatively and CO non-dissociatively.
4. Sketch the molecular orbitals of a free CO molecule and suggest a bonding model for CO molecules adsorbed on a transition metal surface *via* its carbon atom (Hint: the bonding situation is totally analogous to that in transition metal carbonyl complexes – consult textbooks of inorganic or organometallic chemistry for details). Why are bonds between an adsorbed CO molecule and a noble metal (Cu. Ag, Au) surface very weak?

5. Literature

1) M. A. Barteau and R. J. Madix, "The Surface Reactivity of Silver: Oxidation Reactions" in: *The Chemical Physics of Solid Surfaces and Heterogeneous Catalysis, Vol. 4,* D. A. King and D. P. Woodruff, eds., (Elsevier, Amsterdam, Oxford, New York, 1982), 95-142.

2) S. Brunauer, P. H. Emmett, and E. Teller, *J. Am. Chem. Soc.* **60**, 309 (1938).

3) K. Christmann, *Introduction to Surface Physical Chemistry*, (Steinkopff, Darmstadt, 1991).

4) A. Clark, *The Theory of Adsorption and Catalysis*, (Academic Press, London, 1970).

5) A. M. de Jong and J. W. Niemantsverdriet, *Surf. Sci.* **233**, 355-365 (1990).

6) E. Habenschaden and J. Küppers, *Surf. Sci. Lett.* **138**, L147 (1984).

7) I. Langmuir, *J. Am. Chem. Soc.* **40**, 1361 (1918).

8) R. I. Masel, *Principles of Adsorption and Reaction on Solid Surfaces*, (Wiley, New York, 1996).

9) J. W. Niemantsverdriet, *Spectroscopy in Catalysis*, (VCH, Weinheim, 1993).

10) W. Paul, *Z. Physik* **152**, 143 (1958).

11) P. A. Redhead, *Vacuum* **12**, 203-211 (1962).

6. Appendix

K-Type ('T1/T2', 'Chromel/Alumel', 'Ni/NiCr') Thermocouple Characteristics

U [mV]	T [°C]	U [mV]	T [°C]	U [mV]	T [°C]	U [mV]	T [°C]	U [mV]	T [°C]	U [mV]	T [°C]
-6	-207.6	**4**	97.7	**14**	343	**24**	578.8	**34**	817.7	**44**	1070.8
-5.8	-194.3	**4.2**	102.5	**14.2**	347.8	**24.2**	583.5	**34.2**	822.6	**44.2**	1076.1
-5.6	-182.8	**4.4**	107.4	**14.4**	352.6	**24.4**	588.2	**34.4**	827.5	**44.4**	1081.3
-5.4	-172.3	**4.6**	112.2	**14.6**	357.3	**24.6**	592.9	**34.6**	832.4	**44.6**	1086.6
-5.2	-162.8	**4.8**	117.1	**14.8**	362.1	**24.8**	597.6	**34.8**	837.3	**44.8**	1091.9
-5	-153.8	**5**	122	**15**	366.9	**25**	602.3	**35**	842.2	**45**	1097.2
-4.8	-145	**5.2**	126	**15.2**	371	**25.2**	607	**35.2**	847	**45.2**	1102
-4.6	-137.3	**5.4**	131.8	**15.4**	376.4	**25.4**	611.7	**35.4**	852.1	**45.4**	1107.7
-4.4	-129.6	**5.6**	136.7	**15.6**	381.1	**25.6**	616.4	**35.6**	857.1	**45.6**	1113
-4.2	-122.3	**5.8**	141.7	**15.8**	385.9	**25.8**	621.2	**35.8**	862	**45.8**	1118.3
-4	-115.2	**6**	146.6	**16**	390.6	**26**	625.9	**36**	867	**46**	1123.7
-3.8	-108.3	**6.2**	151.6	**16.2**	395.4	**26.2**	630.6	**36.2**	872	**46.2**	1129
-3.6	-101.6	**6.4**	156.5	**16.4**	400.1	**26.4**	635.3	**36.4**	876.9	**46.4**	1134.3
-3.4	-95.1	**6.6**	161.5	**16.6**	404.8	**26.6**	640	**36.6**	881.9	**46.6**	1139.7
-3.2	-88.7	**6.8**	166.5	**16.8**	409.6	**26.8**	644.8	**36.8**	886.9	**46.8**	1145
-3	-82.5	**7**	171.5	**17**	414.3	**27**	649.5	**37**	891.9	**47**	1150.4
-2.8	-76	**7.2**	176	**17.2**	419	**27.2**	654	**37.2**	896	**47.2**	1155
-2.6	-70.4	**7.4**	181.6	**17.4**	423.8	**27.4**	658.9	**37.4**	901.9	**47.4**	1161.2
-2.4	-64.6	**7.6**	186.6	**17.6**	428.5	**27.6**	663.7	**37.6**	906.9	**47.6**	1166.6
-2.2	-58.8	**7.8**	191.6	**17.8**	433.2	**27.8**	668.4	**37.8**	911.9	**47.8**	1172
-2	-53.1	**8**	196.6	**18**	437.9	**28**	673.2	**38**	916.9	**48**	1177.4
-1.8	-47.5	**8.2**	201.6	**18.2**	442.6	**28.2**	677.9	**38.2**	922	**48.2**	1182.9
-1.6	-42	**8.4**	206.6	**18.4**	447.3	**28.4**	682.7	**38.4**	927	**48.4**	1188.3
-1.4	-36.6	**8.6**	211.6	**18.6**	452	**28.6**	687.4	**38.6**	932	**48.6**	1193.8
-1.2	-31.2	**8.8**	216.6	**18.8**	456.8	**28.8**	692.2	**38.8**	937.1	**48.8**	1199.2
-1	-25.9	**9**	221.5	**19**	461.5	**29**	696.9	**39**	942.2	**49**	1204.7
-0.8	-20	**9.2**	226	**19.2**	466	**29.2**	701	**39.2**	947	**49.2**	1210
-0.6	-15.4	**9.4**	231.5	**19.4**	470.9	**29.4**	706.5	**39.4**	952.3	**49.4**	1215.7
-0.4	-10.2	**9.6**	236.4	**19.6**	475.6	**29.6**	711.3	**39.6**	957.4	**49.6**	1221.2
-0.2	-5.1	**9.8**	241.4	**19.8**	480.3	**29.8**	716.1	**39.8**	962.5	**49.8**	1226.8
0	0	**10**	246.3	**20**	485	**30**	720.8	**40**	967.6	**50**	1232.3
0.2	5	**10.2**	251.2	**20.2**	489.7	**30.2**	725.6	**40.2**	972.7	**50.2**	1237.9
0.4	10.1	**10.4**	256.1	**20.4**	494.4	**30.4**	730.4	**40.4**	977.8	**50.4**	1243.5
0.6	15.1	**10.6**	261	**20.6**	499.1	**30.6**	735.2	**40.6**	982.9	**50.6**	1249.1
0.8	20	**10.8**	265.9	**20.8**	503.8	**30.8**	740	**40.8**	988	**50.8**	1254.7
1	25	**11**	270.8	**21**	508.5	**31**	744.8	**41**	993.1	**51**	1260.3
1.2	29	**11.2**	275	**21.2**	513	**31.2**	749	**41.2**	998	**51.2**	1265
1.4	34.8	**11.4**	280.5	**21.4**	517.8	**31.4**	754.5	**41.4**	1003.4	**51.4**	1271.6
1.6	39.7	**11.6**	285.3	**21.6**	522.5	**31.6**	759.3	**41.6**	1008.5	**51.6**	1277.3
1.8	44.6	**11.8**	290.2	**21.8**	527.2	**31.8**	764.1	**41.8**	1013.7	**51.8**	1282.9
2	49.5	**12**	295	**22**	531.9	**32**	769	**42**	1018.8	**52**	1288.6
2.2	54.3	**12.2**	299.8	**22.2**	536.6	**32.2**	773.8	**42.2**	1024	**52.2**	1294.3
2.4	59.1	**12.4**	304.6	**22.4**	541.3	**32.4**	778.7	**42.4**	1029.2	**52.4**	1300.1
2.6	64	**12.6**	309.4	**22.6**	546	**32.6**	783.5	**42.6**	1034.4	**52.6**	1305.8
2.8	68.8	**12.8**	314.3	**22.8**	550.7	**32.8**	788.4	**42.8**	1039.6	**52.8**	1311.5
3	73.6	**13**	319.1	**23**	555.4	**33**	793.3	**43**	1044.8	**53**	1317.3
3.2	78	**13.2**	323	**23.2**	560	**33.2**	798	**43.2**	1050	**53.2**	1323
3.4	83.2	**13.4**	328.7	**23.4**	564.7	**33.4**	803	**43.4**	1055.2	**53.4**	1328.9
3.6	88	**13.6**	333.4	**23.6**	569.4	**33.6**	807.9	**43.6**	1060.4	**53.6**	1334.7
3.8	92.9	**13.8**	338.2	**23.8**	574.1	**33.8**	812.8	**43.8**	1065.6	**53.8**	1340.5
4	97.7	**14**	343	**24**	578.8	**34**	817.7	**44**	1070.8	**54**	1346.4